H_2 dissociative adsorption on Pd(111)

W. Dong
Institut de Recherches sur la Catalyse, Centre National de la Recherche Scientifique, 2, Avenue Albert Einstein, F-69626 Villeurbanne Cedex, France
and Ecole Normale Supérieure de Lyon, 46, allée d'Italie, F-69364 Lyon Cedex 07, France

J. Hafner
Institut für Theoretische Physik, Technische Universität Wien, Wiedner Hauptstrasse 8-10, A-1040 Wien, Austria
(Received 5 May 1997)

The dissociative adsorption of hydrogen molecules on the (111) surface of palladium is studied by total-energy calculations using the density-functional theory within the framework of the generalized gradient approximation. A variety of dissociation pathways is investigated. Both activated and nonactivated pathways are found. We carry out a detailed analysis of the electronic structure along the different pathways to understand the microscopic mechanism of bond breaking and bond formation. This analysis allows us to account for the energetic ordering of the transition states. Precursor states are also identified for the system considered here. [S0163-1829(97)03148-2]

I. INTRODUCTION

Dissociative adsorption of hydrogen on metal surfaces can serve as the simplest prototype of chemical reactions on the metal surfaces. The understanding of the dissociative adsorption process over various metal surfaces will give insights into the heterogeneous catalysis of more complex systems. The hydrogen-palladium system is one of the extensively studied systems due to its importance in a variety of technological applications. For example, palladium can be used as catalyst for hydrogenation reactions of the Fischer-Tropsch type. The dissociative adsorption of H_2 on the surface of a catalyst is the first elementary step of such reactions. Now, a large amount of experimental informations is available for the hydrogen-palladium system under well-controlled conditions thanks to the high vacuum techniques. Early experimental efforts have been focused on characterizing the atomic chemisorption of H on various low-index surfaces of palladium.[1–15] One important general feature found from these experiments is that the most favorable adsorption site is that with a high coordination number. In the case of Pd(111), it is the threefold hollow site. Low-energy-electron-diffraction measurements[3–7] have characterized the geometric structure of the adsorption site. The electronic structures of the clean and hydrogen-covered palladium surfaces have been investigated by means of ultraviolet photoelectron spectroscopy and electron-energy-loss spectroscopy.[11–15] The dynamics of dissociative adsorption has been studied with molecular-beam techniques.[16–21] Two classes are found for the behaviors of the sticking probability. In the first one, the sticking probability is a monotonically increasing function of the kinetic energy of the impinging molecules. This feature is associated with activated dissociations. In the second class, the sticking probability decreases first in the low incident energy region and then increases with the beam energy. This behavior was attributed to the existence of both activated and nonactivated pathways and/or to the existence of molecularly adsorbed precursor states before dissociation. While this picture can account for the initial decrease of the sticking probability, no direct experimental determination of such precursor states has been reported. Moreover, the precise conditions under which the steering effect and the precursor effect come into play are not yet elucidated. For example, quite different dynamic behaviors have been found for the H_2 dissociation on Pt(111) and Ni(111) (no initial decrease of the sticking probability) compared to Pd(111).[19] This has been attributed to the lack of precursor state. However, it can be expected that nonactivated paths exist on Pt(111) and Ni(111) for the dissociation of H_2. Why the steering effect does not seem to operate here? To answer this question, thorough investigations should be carried out in parallel for H_2/Pd(111), H_2/Pt(111), and H_2/Ni(111).

Theoretical studies have been also carried out for the chemisorption of atomic hydrogen on various palladium surfaces.[22–33] Early work was based on semiempirical approaches like embedded-cluster[22,23] or embedded-atom[24] methods and effective-medium models.[25] *Ab initio* calculations have been carried out also[26–33] that provide an accurate description of the main features of chemisorption on a variety of metal surfaces. Very recently, *ab initio* approaches have been applied to study the dissociative adsorption of H_2 on a variety of transition- and noble-metal surfaces.[34–45] The potential energy surfaces (PES) determined from these *ab initio* calculations allow to carry out classic and quantum dynamic simulations of the adsorption process.[46–48] These investigations of the dynamics reveal translational and orientational steering effects driving the H_2 molecule into favorable pathways in the low beam energy regime. For the systems studied up to now, no evidence has been found for the existence of precursor states.

In this paper, we present a detailed study of the dissociative adsorption of H_2 on the Pd(111) surface by *ab initio* calculations. A variety of dissociation pathways is examined. Both activated and nonactivated pathways are found depending on the impinging point of the adsorbate molecule on the

surface. We carefully analyze the electronic structure. This allows to understand why some pathways are activated and the others are not. Precursor states are also found for the system considered here.

II. METHOD

The calculations presented in this work have been carried out using the Vienna *ab initio* simulation program (VASP).[49–52] VASP performs an iterative solution of the Kohn-Sham equations of density-functional theory using residuum-minimization methods or sequential band-by-band conjugate gradient techniques and optimized charge-density mixing routines.[51,52] We use the exchange-correlation functional based on the quantum Monte Carlo simulations of Ceperley and Alder[53] as parameterized by Perdew and Zunger.[54] The correction based on the generalized gradient approximation (GGA) proposed by Perdew and Wang[55] is also included. In our calculations, GGA is included in the self-consistent procedure, i.e., not only a GGA correction based on the local density approximation (LDA) electron density being added. The valence orbitals are expanded in a plane-wave basis, with the electron-ion interaction described by the ultrasoft pseudopotentials proposed by Vanderbilt[56] and optimized by Kresse and Hafner.[57] The pseudopotentials used here have been described in details in the previous work on the atomic chemisorption of H on Pd(111).[32] Thanks to the efficiency of the ultrasoft pseudopotentials, the plane-wave expansion of the valence wave functions can be truncated at the cutoff energy of 200 eV that leads to 1 mRy convergence for the cohesive and adsorption energies. Brillouin-zone integrations have been performed on a grid of special Monkhost-Pack points,[58] using a Gaussian smearing with a width of 0.4 eV for the one-electron levels within the generalized finite-temperature density-functional theory (see Refs. 51 and 52 for details). To model a surface, we adopt the slab supercell approach. All the calculations presented in this work are made on a slab containing five palladium layers. A vacuum space corresponding to five Pd layers is used to separate the central slab and its periodic images. During the adsorption, the substrate is kept at the truncated bulk geometry with the calculated equilibrium lattice constant. This rigid substrate model can be justified by the fact that Pd atoms and the H_2 molecule have very different time scales due to the large mass difference between them and the surface Pd layer undergoes a very small relaxation.[32] All the calculations are made with a $\sqrt{3}\times\sqrt{3}$ surface cell (see Fig. 1). At low temperatures, the $c(\sqrt{3}\times\sqrt{3})R30°$ chemisorption pattern of H on Pd(111) has been identified experimentally.[9,10] One dissociation pathway studied in this work leads directly to this chemisorption pattern.

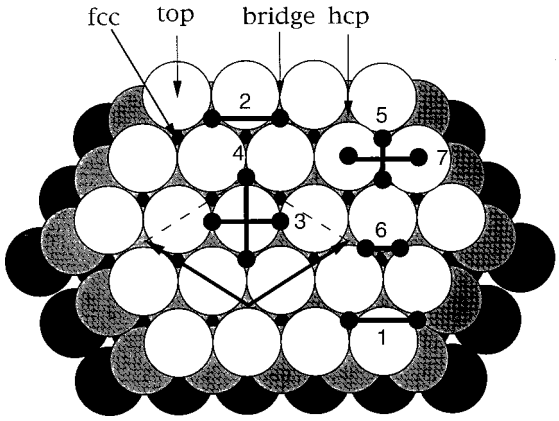

FIG. 1. Schematic presentation of a (111) surface showing the different adsorption sites and the end configurations of the dissociative adsorption: (1) fcc-fcc; (2) hcp-hcp; (3) *b*-*t*-*b* (bridge-top-bridge); (4) fcc-*t*-hcp; (5) fcc-hcp; (6) bridge-bridge; (7) top-top.

III. RESULTS AND DISCUSSIONS

A. End configurations of different pathways

We will first summarize some calculated properties of the adsorbate and the substrate and of the end configurations of the different pathways to be considered in the following. Within GGA, we found a bulk lattice constant of $a = 3.95$ Å which is slightly larger than our previous LDA result of 3.88 Å,[32] but still in good agreement with the experimental value of 3.89 Å.[59] The bond length of H_2 given by our GGA calculation is 0.75 Å, in good agreement with the experimental value of 0.74 Å. In our previous work,[32] the chemisorption of atomic H on Pd(111) has been studied for the coverages at 1 (ML) and 1/4 ML. For the $\sqrt{3}\times\sqrt{3}$ surface cell used in this work, the adsorption of H_2 leads to a coverage of 2/3 ML. The end configurations of the different reaction paths considered are depicted in Fig. 1. The adsorption energies and geometries of these end configurations are summarized in Table I. Among the considered configurations, only the top-top configuration is unstable against dissociation. Here, we recover the energetic ordering of different adsorption sites already known from the atomic chemisorption study.[32] The threefold hollow sites are the most stable with the fcc site being slightly more stable than the hcp site. However, the fcc-hcp and fcc-*t*-hcp configurations are less stable by about 100 meV than the fcc-fcc and hcp-hcp configurations. This destabilization is due to the fact that there is one H-H distance equal only to 1.61 Å in the fcc-hcp and fcc-*t*-hcp configurations, leading to a strong repulsion between H atoms. The same kind of destabilization

TABLE I. Adsorption energy E_{ad} and geometries of end configurations, $\theta = \frac{2}{3}$ ML.

Configuration	fcc-fcc	hcp-hcp	*b*-*t*-*b*	fcc-*t*-hcp	fcc-hcp	bridge-bridge	top-top
E_{ad} (eV/atom-H)[a]	−0.498	−0.446	−0.329	−0.347	−0.347	−0.191	0.162
$d_{H\text{-}H}$ (Å)	2.79	2.79	2.79	2.79	1.61	1.40	2.79
h_H (Å)	0.84	0.84	1.01	0.83	0.83	1.04	1.55
$d_{H\text{-}Pd}$ (Å)	1.82	1.82	1.72	1.81	1.81	1.74	1.55

[a] $E_{ad} = (E[H_2/Pd(111)] - E[H_2] - E[Pd(111)])/N_H$.

arises also in the bridge-bridge configuration, leading to an energy-increase of 138 meV compared to the *b-t-b* configuration.

B. Dissociative adsorption pathways and potential energy surface

Within the Born-Oppenheimer and rigid-substrate approximations, all the dynamic informations about the dissociative adsorption can be obtained in principle from the six-dimensional potential energy surface. However, the direct determination of such a hypersurface remains a daunting task. Therefore, we have to appeal to our physical and chemical intuition for selecting some plausible low-energy paths in a more restricted space. These different paths constitute low-dimensional cuts of the 6D PES. From these low-dimensional cuts, an approximate 6D PES can be built by interpolation, which allows dynamic calculations to be carried out.[44,46,47] We know that the dissociation process costs less energy if the bond breaking of the hydrogen molecule is accompanied by the simultaneous formation of a strong adsorbate-substrate bond. Based on this argument, one assumes that the pathways in which the hydrogen molecule remains essentially parallel to the surface with the atoms orientated towards high-symmetry sites are the energetically favorable ones. In their recent works on the dissociative adsorption of H_2 on the (100) surface of Rh, Pd, and Ag, Wilke and Scheffler[41] and Eichler, Kresse, and Hafner[42,43] have shown that a cartwheel rotation (a rotation moving the hydrogen molecule out of a plane parallel to the surface) gives rise to a sharp increase of energy. Hence, in the present work we will restrict ourselves considering only pathways in which the hydrogen molecule approaches the surface with its molecular axis parallel to the surface.

In total, we have studied seven different dissociation pathways. We name these pathways by their end configurations. The geometry of these pathways is shown in Fig. 1. The selection of these pathways constitutes a representative sampling with different molecular orientations and locations of the center of mass in the unit cell. This will hopefully supply sufficient information for building the higher-dimensional PES by interpolation. Among the seven dissociation pathways, four lead the H_2 molecule to dissociate directly to hollow sites, i.e., fcc-fcc, hcp-hcp, fcc-*t*-hcp, and fcc-hcp paths. In the nomenclature of these dissociation pathways, the sites for which head the two H atoms are given explicitly and for the path names with three items, e.g., fcc-*t*-hcp; the middle one specifies the position of the center of mass. Two paths considered here bear some resemblance to two of those studied by Wilke and Scheffler[41] and Eichler, Kresse, and Hafner,[42,43] for the dissociation of H_2 on the (100) surface in the sense that along the fcc-hcp path, the center of mass of H_2 is over the bridge site with the two H atoms dissociating into two hollow sites and along fcc-*t*-hcp path, the center of mass of H_2 locates at the top site with two H atoms dissociating into two hollow sites. There are two paths leading to the dissociation into two bridge sites, i.e., the *b-t-b* and bridge-bridge paths and one path to two top sites, i.e., the top-top path.

The 2D cuts of the seven dissociation pathways are plotted in Fig. 2. These ''elbow'' plots are obtained by interpolating about 60 calculated points scanning different bond lengths of H_2, $d_{\mathrm{H\text{-}H}}$, and the height of the center of mass above the surface z. Figure 2(h) shows in addition the variation of the energy at the bottom of each reaction path as a function of the distance from the surface. From these plots, one can see that four dissociation pathways are nonactivated: the fcc-fcc, hcp-hcp, *b-t-b*, and fcc-*t*-hcp paths. However, for none of these paths the potential energy decreases monotonically along the reaction coordinate. This is similar as along the *b-t-b* dissociation path on Pd(100).[42,43] In contrast, the potential energy decreases monotonically along the other nonactivated pathways for the dissociation of H_2 on Pd(100).[41] The most favorable dissociation pathway is the fcc-fcc path. There are two transition states (TS) along this path. The first is an unimportant one. By this, we mean that this first TS does not characterize the bond breaking of the H_2 molecule. After this first TS, there is a precursor state. We will come back later to discuss the very existence of the precursor state. The bond breaking of the H_2 molecule is characterized by the second TS. This TS gives a barrier of 115 meV with respect to the precursor state but it is still lower by 95 meV compared to the noninteracting H_2 and Pd(111) [see Fig. 2(h)]. This TS is a late one in the exit channel. The H-H bond is stretched to 1.06 Å. The TS is at a quite short distance to the surface, $z = 1.38$ Å. The hcp-hcp path is similar to the fcc-fcc path in nearly all the aspects [see Fig. 2(b) and Table II]. This resemblance is expected from the similarity between the geometries of the two paths and that between the fcc and hcp sites. The second TS on the hcp-hcp path is about 20 meV higher than the corresponding TS on the fcc-fcc path. This correlates well with the fact that the fcc site is slightly more favorable than the hcp site.

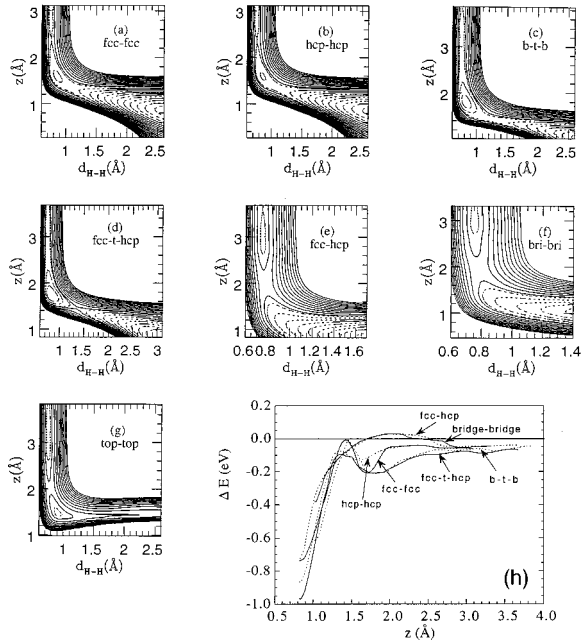

FIG. 2. 2D cuts of PES for different dissociation pathways: (a) fcc-fcc; (b) hcp-hcp; (c) *b-t-b*; (d) fcc-*t*-hcp; (e) fcc-hcp; (f) bridge-bridge; (g) top-top; (h) energy variation on the bottom of different paths. Contours in full line correspond to positive values and those in dashed line to negative values. Contour spacing is 80 meV/molecule.

TABLE II. Transition states along dissociation pathways, $\theta=\frac{2}{3}$ ML.

Pathway	fcc-fcc	hcp-hcp	*b-t-b*	fcc-*t*-hcp	fcc-hcp	bridge-bridge	top-top
ΔE (eV)[a]	−0.095	−0.074	−0.005	−0.002	0.019	0.021	0.012
$d_{\text{H-H}}$ (Å)	1.06	1.08	1.35	1.35	0.78	0.79	0.78
h_{H} (Å)	1.38	1.37	1.45	1.45	1.93	1.93	2.01
$d_{\text{H-Pd}}$ (Å)	1.68	1.68	1.60	1.60	2.42	2.31	2.25

[a]Noninteracting H_2 and Pd(111) as energy reference.

The other two nonactivated dissociation pathways are the *b-t-b* and fcc-*t*-hcp paths. For both configurations, the center of gravity of the molecule is located on top of a Pd atom. The orientations of the H_2 molecule in these two paths are perpendicular to each other (see Fig. 1). These two paths are nearly identical. First, the adsorbate encounters a precursor state with a depth of about 210 meV and then a TS which is still slightly more stable by a few meV than the noninteracting molecule and surface (see Tables II and III). The TS is found in the exit channel and the H-H bond is more stretched than in fcc-fcc and hcp-hcp paths (see Table II). This accounts for the higher energy at this TS. The close likeness between the *b-t-b* and fcc-*t*-hcp paths shows that an in-plane rotation on the top site is almost free. This is in contrast to the (100) surface where large differences in the energies of *h-t-h* and *b-t-b* configurations at constant height have been found.[42,43]

The fcc-hcp and bridge-bridge paths are two activated dissociation pathways. They share some common features. There is no precursor state along these paths and the TS's along both the paths are located in the entrance channel (early TS) with the H-H bond being stretched only by 0.03 Å compared to the bond length of the free molecule. A well-known rule of thumb in chemistry states that an early TS corresponds to a low-energy barrier. In terms of the H-H bond stretching, the TS's along the four nonactivated pathways are all much later than the TS's along the fcc-hcp and bridge-bridge paths (see Table II). However, it should be noted that the TS's along these latter two ones are more distant from the surface. The fcc-hcp path studied here resembles somehow the *h-b-h* path on Pd(100) studied in Refs. 41–43 in the sense that these paths are all located over a bridge site and lead to the dissociation into two hollow sites. While such a path is nonactivated for the dissociation of H_2 on Pd(100),[41] it is activated on Pd(111). Although the fcc-hcp and bridge-bridge paths are activated ones, the required activation energies are quite small (about 20 meV). These barrier heights are comparable to those found along the *h-b-h* dissociation path on the (100) surface of Pd and Rh (10 and 20 meV, respectively). A much higher barrier is found, however, along the *b-h-b* path on Pd(100) (90 meV).[43]

TABLE III. Energies and geometries of precursor states.

Pathway	fcc-fcc	hcp-hcp	*b-t-b*	fcc-*t*-hcp
ΔE (eV)[a]	−0.210	−0.116	−0.213	−0.211
$d_{\text{H-H}}$ (Å)	0.83	0.86	0.82	0.84
h_{H} (Å)	1.75	1.59	1.80	1.74

[a]Noninteracting H_2 and Pd(111) as energy reference.

Finally, the top-top path does not lead to dissociative adsorption. From Fig. 2(g), we see that along this path there is a very shallow potential well. After this well, the stretching of H-H bond causes the energy to increase continuously and leads to an end-configuration unstable with respect to the noninteracting H_2 and Pd(111) (see Table I).

Now, let us come back to discuss in some details the precursor states. The existence of precursor states has been postulated as a possible explanation for the decrease of sticking coefficient with the increase of incident beam energy in the low-energy regime. To our knowledge, the very existence of precursor state has never been directly determined from experiments. In the work of Wilke and Scheffler[41] on the dissociation of H_2 on Pd(100), there seems to appear some sign for the existence of precursor state along a *h-t-h* dissociation path over the top site. Nevertheless, they have checked that the potential well before the TS does not correspond to a local minimum of the PES. Its presence is due to the restriction for the motion of the center of mass of the molecule. If it is allowed to relax, the dissociation takes place along a purely attractive path by sliding away from the top site when approaching more and more the surface. This behavior has also shown clearly for the dissociation of H_2 on the (100) surface of Rh, Pd, and Ag in the recent works of Eichler, Kresse, and Hafner.[42,43] Hence, no precursor state exists on the (100) surface of Pd and Rh. The quantum dynamic simulation of Gross, Wilke, and Scheffler[47] have demonstrated that the observed nonmonotonic behavior of the sticking coefficient arises from the simultaneous presence of nonactivated and activated reaction pathways leading to dynamic stearing effects whose efficiency in increasing the sticking probability depends on the kinetic energy. To make sure that the potential wells before TS's along the fcc-fcc, hcp-hcp, *b-t-b*, and fcc-*t*-hcp paths correspond really to precursor states, we have carried out calculations at these positions, relaxing all the six degrees of freedom of the H_2 molecule. The results show that they are all the true local minima of the PES. So precursor states indeed exist for the dissociation of H_2 on Pd(111). The existence of the precursor state makes the dissociation of H_2 over the top site on Pd(111) somewhat different from that happening on Pd(100) and Rh(100). On Pd(100) and Rh(100), the H_2 molecule initially centered at the top position will slide away when approaching more and more the surface. This sliding takes place spontaneously without any energy barrier and the dissociation follows a purely attractive path. If there were no precursor state on Pd(111), the *b-t-b* path would be able to join gradually the fcc-fcc or the hcp-hcp path by parallel sliding without activation when H_2 approaches more and more the surface. However, we have found that there is an energy barrier for such a sliding. The results for the precur-

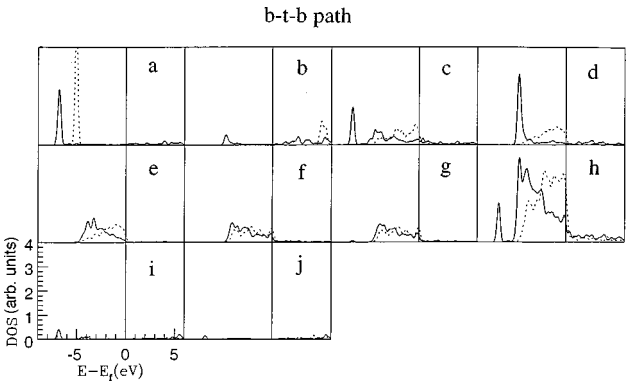

FIG. 3. Density of states at the TS on *b-t-b* path projected on the following orbitals: (a) σ; (b) σ^*; (c) $d_{3z^2-r^2}$; (d) d_{xz}; (e) d_{yz}; (f) d_{xy}; (g) $d_{x^2-y^2}$; (h) total *d* band; (i) *s*; (j) p_z. DOS in full line is for H_2 on Pd(111) and that in dashed line for the noninteracting H_2 and Pd(111).

sor states are summarized in Table III. These precursor states should be qualified as chemisorbed molecular states in which there are already significant binding with the substrate and non-negligible stretching of the H-H bond length.

C. Chemical bond breaking and forming—electronic structure

The breaking and forming of chemical bonds result from the electronic reorganization between reactants, i.e., the adsorbate and the substrate in the case of dissociative adsorption. Thus, the analysis of the electronic structure changes accompanying the dissociative adsorption process furnishes valuable insights into the microscopic mechanism.[60,61] The electronic reorganization manifests itself through the modification of the density of states (DOS) projected on the orbitals involved in the adsorbate-substrate interactions.[36,37,42,43,60,61] In the followings, we will analyze the electronic reorganization along the dissociation paths presented in the last subsection. The transition state is a characteristic point for the H-H bond breaking and the adsorbate-substrate bond formation. All the projected DOS's presented here are made at the transition states (see Ref. 62 for some details of angular projections).

Now, let us start with the *b-t-b* pathway. In Fig. 3, the projected DOS's presented in full line are those at the TS and those in dashed line for the noninteracting H_2 molecule and the Pd(111) substrate. The comparison between them shows clearly the orbitals involved in the interaction. The bonding level of the H_2 molecule σ is shifted to a lower energy due to its interaction with the $d_{3z^2-r^2}$, *s* and p_z bands of the substrate. The largest interaction is that between σ and $d_{3z^2-r^2}$. At the TS, the antibonding state of the H_2 molecule σ^* starts to be filled due to its interaction with the d_{xz} band [see Fig. 3(b)]. This interaction transforms the initially broad d_{xz} band into a quite narrow peak located at the bottom of the *d* band [see Fig. 3(d)]. In summary, the main feature of the electronic structure at this TS is a split-off peak appearing below the *d* band due to essentially the interaction between σ and $d_{3z^2-r^2}$ and an important depletion of the *d* band near the Fermi level with increasing populations at the bottom of the *d* band. The deformation of the *d* band [see Fig. 3(h)] results mainly from the σ^*-d_{xz} and $\sigma-d_{3z^2-r^2}$ interactions. For

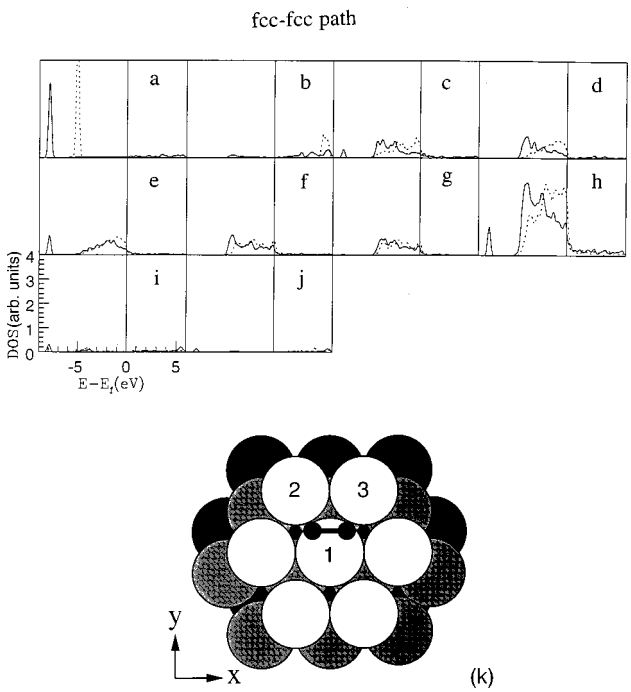

FIG. 4. Density of states at the TS on fcc-fcc path projected on the following orbitals: (a) σ; (b) σ^*; (c) $d_{3z^2-r^2}$; (d) d_{xz}; (e) d_{yz}; (f) d_{xy}; (g) $d_{x^2-y^2}$; (h) total *d* band; (i) *s*; (j) p_z; (k) Sketch of the TS geometry. DOS in full line is for H_2 on Pd(111) and that in dashed line for the noninteracting H_2 and Pd(111).

the fcc-*t*-hcp path, the electronic structure at the TS is essentially the same as that we have just seen. This is expected since the two TS's are very similar. The only difference is that for the fcc-*t*-hcp path, σ^* interacts with d_{yz} instead of d_{xz} since on this path the H_2 molecule is rotated by 90° with respect to the *b-t-b* path (see Fig. 1). We will not reproduce here the extremely similar projected DOS's for the fcc-*t*-hcp path.

In Fig. 4, the projected DOS's at the TS for the fcc-fcc path are presented. On the fcc-fcc path, the H_2 molecule is displaced in the *y* direction by 0.81 Å compared to its position on the *b-t-b* path [see the sketch in Fig. 4(k)]. At the TS of this path, the H_2 molecule interacts significantly only with the atom Pd(1) [see Fig. 4(k)]. Hence, the projected DOS's for the substrate presented in Fig. 4 are those located at Pd(1). As on the *b-t-b* path, the bonding σ orbital of H_2 interacts with the $d_{3z^2-r^2}$, *s*, and p_z bands and the antibonding σ^* orbital interacts with the d_{xz} band. The σ^*-d_{xz} interaction is weaker than on the *b-t-b* path because the orbital overlap is decreased due to the sliding away from Pd(1). The weaker interaction between σ^* and d_{xz} can be seen from the DOS's projected on these orbitals and comparing them with the corresponding projected DOS's on the *b-t-b* path. A new feature appearing here is that the σ orbital can now also interact with the d_{yz} orbital on Pd(1) [see Fig. 4(e)]. This interaction is forbidden on the *b-t-b* path by the orbital symmetries. This can help to understand why the TS on the fcc-fcc path is lower in energy than that on the *b-t-b* path. On the fcc-fcc path, the σ orbital of H_2 interacts less well with the $d_{3z^2-r^2}$ orbital on Pd(1) than on the *b-t-b* path. Nevertheless, this $\sigma-d_{3z^2-r^2}$ interaction is still significant and, moreover, the $\sigma-d_{yz}$ interaction comes into play. These two

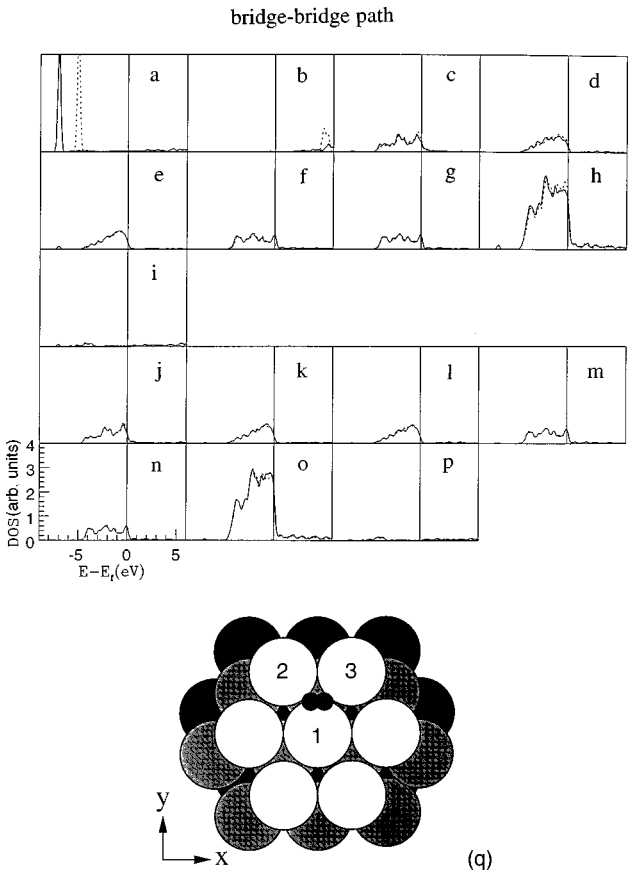

FIG. 5. Density of states at the TS on bridge-bridge path projected on the following orbitals: (a) σ; (b) σ^*; (c) $d_{3z^2-r^2}$; (d) d_{xz}; (e) d_{yz}; (f) d_{xy}; (g) $d_{x^2-y^2}$; (h) total d band; (i) s. The projections shown in c to i are located on Pd(1) and those in j to p are the same projections but located on Pd(2). (q) Sketch of the TS geometry. DOS in full line is for H_2 on Pd(111) and that in dashed line for the noninteracting H_2 and Pd(111).

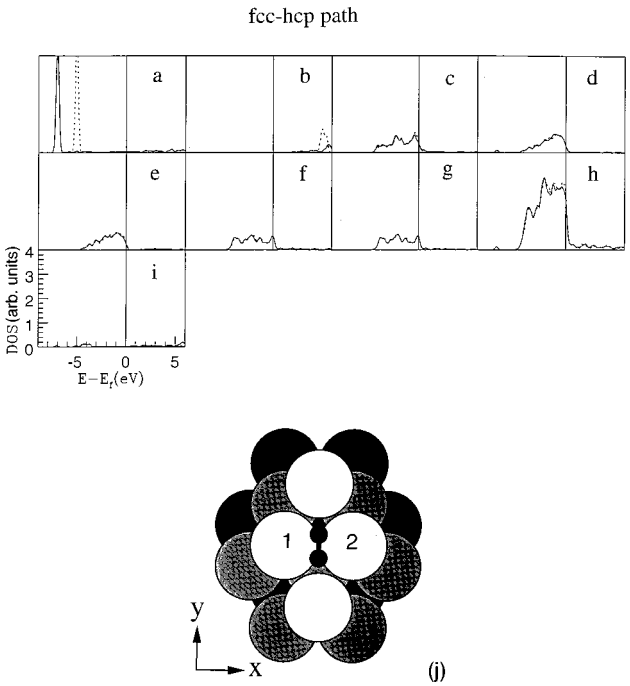

FIG. 6. Density of states at the TS on fcc-hcp path projected on the following orbitals: (a) σ; (b) σ^*; (c) $d_{3z^2-r^2}$; (d) d_{xz}; (e) d_{yz}; (f) d_{xy}; (g) $d_{x^2-y^2}$; (h) total d band; (i) s; (j) Sketch of the TS geometry. DOS in full line is for H_2 on Pd(111) and that in dashed line for the noninteracting H_2 and Pd(111).

interactions together make a larger stabilization. The electronic structure of the TS on the hcp-hcp path is essentially the same as that on the fcc-fcc path. Hence, the projected DOS's for the hcp-hcp pathway will not be shown.

On the bridge-bridge path, the H_2 molecule is moved still a little bit further away from Pd(1) [see the sketch in Fig. 5(q)]. The orbital interaction between σ and $d_{3z^2-r^2}$ on Pd(1) nearly disappears [see Fig. 5(c)]. There are only very weak interactions between σ and d_{yz} and s bands [see Figs. 5(e) and 5(i)]. At the TS on this path, σ^* does not play any role in orbital interactions [see Fig. 5(b)]. Even at this TS, no interaction is found with Pd(2) and Pd(3). This is shown clearly by Figs. 5(j)–(p) which display the projected DOS's located on Pd(2). One sees hardly modifications with respect to the clean Pd(111) surface. The very week orbital interaction at the TS accounts well for the fact that the bridge-bridge path is an activated one.

The electronic structure at the TS on the fcc-hcp path is quite similar to that of the bridge-bridge path. There are only very weak interactions of σ with d_{xz} and s orbitals and σ^* does not enter into any interaction (see Fig. 6). Since the top-top path does not lead to a stable dissociation state, we will not present its electronic structure. We point out just that there are only extremely week orbital interactions. From all these results, we see that there exists a correlation between the filling of the σ^* orbital and the bond stretching of H_2 at the TS: the more σ^* is occupied the more the H-H bond is stretched. This is just the very mechanism of the bond breaking. Comparing our results with those obtained for the (100) surface,[41–43] we find that on the more compact (111) surface the corrugation experienced by the impinging molecule is much less pronounced. This reduced corrugation is reflected by a less pronounced variation of energies of the different pathways located on different positions of the substrate.

IV. CONCLUSION

In the present work, we have studied the dissociative adsorption of H_2 on Pd(111) by applying a pseudopotential-based *ab initio* density functional technique within the framework of the generalized gradient approximation. A variety of dissociation pathways with different impinging points and different azimuthal orientations is investigated. Among the considered pathways only one, the top-top path, does not lead to a stable dissociation state and all the others are either nonactivated or slightly activated with activation energies of about 20 meV. Hence, these results show that Pd(111) can dissociate H_2 molecules quite efficiently. This agrees fairly well with the quite large sticking coefficient of H_2 on Pd(111) found experimentally. Precursor states have been identified, representing chemisorbed molecular states in which there is already significant binding with the substrate and appreciable bond stretching of the H_2 molecule. The precursor states found here have well depths of about 100–200 meV. These are in very good agreement with the experimental result[19] for the beam energy at which the sticking prob-

ability is minimum (this beam energy is usually considered as a measure of the well depth of precursor states). The precursor states we have found here differ from what was believed about a precursor state—a quite uniform potential well in front of the surface depending little on the point of impact of the adsorbate. In fact, our results show that precursor states are corrugated also. Therefore, even in the presence of precursor states, dynamic steering effects will still play an important role in driving the adsorbate into favorable reaction pathways. The simultaneous presence of nonactivated paths and precursor states makes the system we have studied here a quite unique one for studying in details the dynamic mechanics of dissociative adsorption. Up to now, two effects are considered to be the cause for the initial decrease of the sticking probability as function of beam energy. However, the precise role of each effect is not so clear, for example, a powerful method is still lacking for distinguishing these two effects from each other. Therefore, further investigations on dynamics are expected to make progresses in this direction. The results obtained in this work supply the prerequisite informations for building the PES needed in such investigations. We have also analyzed in details the electronic structure at the transition state along the different pathways to understand the microscopic mechanism of bond breaking and formation. This analysis allows to account for the energetic ordering of the different TS's. At the TS's considered here, the main role is played by the interaction of the σ-bonding orbital of H_2 with the d orbitals of the substrate. The filling of the antibonding σ^* molecular orbital correlates with the bond stretching of H_2 at the transition state. This is nothing but the microscopic mechanism of the bond breaking. The high-dimensional PES can be constructed from the results obtained in this work which will allow dynamic simulations to be carried out. Work in this direction is being undertaken.

ACKNOWLEDGMENTS

Computer time on the Cray C98 was allocated for the present work by IDRIS du Centre National de la Recherche Scientifique through project No. 950609. This work has been undertaken within the GdR-Dynamique Moléculaire Quantique Appliquée à la Catalyse, a joint project of CNRS, the Technische Universität Wien, and the Institut Français du Pétrole.

[1] K. Christmann, in *Hydrogen Effects in Catalysis*, edited by Z. Paál and P. G. Menon (Marcel Dekker, Inc., New York, 1988).
[2] K. Christmann, Surf. Sci. Rep. **9**, 1 (1988).
[3] K. Christmann, G. Ertl, and D. Schober, Surf. Sci. **40**, 61 (1973).
[4] H. Conrad, G. Ertl, and E. E. Latta, Surf. Sci. **41**, 435 (1974).
[5] M. G. Cattania, V. Penka, R. J. Behm, K. Christmann, and G. Ertl, Surf. Sci. **126**, 382 (1983).
[6] H. Ohtani, M. A. Van Hove, and G. A. Somorjai, Surf. Sci. **187**, 372 (1987).
[7] T. E. Felter, E. G. Sowa, and M. A. Van Hove, Phys. Rev. B **40**, 891 (1989).
[8] C. J. Barnes, M. Q. Ding, M. Lindroos, R. D. Diehl, and D. A. King, Surf. Sci. **162**, 59 (1985).
[9] T. E. Felter and R. H. Stulen, J. Vac. Sci. Technol. A **3**, 1566 (1985).
[10] T. E. Felter, S. M. Foiles, M. S. Daw, and R. H. Stulen, Surf. Sci. **171**, L379 (1986).
[11] H. Conrad, G. Ertl, J. Küppers, and E. E. Latta, Surf. Sci. **58**, 578 (1976).
[12] J. E. Demuth, Surf. Sci. **65**, 369 (1977).
[13] W. Eberhardt, F. Greuter, and E. W. Plummer, Phys. Rev. Lett. **46**, 1085 (1981).
[14] W. Eberhardt, S. G. Louie, and E. W. Plummer, Phys. Rev. B **28**, 465 (1983).
[15] F. P. Netzer and M. M. El Gomati, Surf. Sci. **124**, 26 (1983).
[16] K. D. Rendulic, G. Anger, and A. Winkler, Surf. Sci. **208**, 404 (1989).
[17] K. Schmidt, T. Schlathölter, A. Närmann, and W. Heiland, Chem. Phys. Lett. **200**, 465 (1992).
[18] K. D. Rendulic, Surf. Sci. **272**, 34 (1992).
[19] Ch. Resch, H. F. Berger, K. D. Rendulic, and E. Bertel, Surf. Sci. **316**, L1105 (1994).
[20] K. D. Rendulic and A. Winkler, Surf. Sci. **299/300**, 261 (1994).
[21] M. Beutl, M. Riedler, and K. D. Rendulic, Chem. Phys. Lett. **247**, 249 (1995).
[22] J. P. Muscat and D. M. Newns, Surf. Sci. **80**, 189 (1979).
[23] J. P. Muscat, Surf. Sci. **110**, 85 (1981).
[24] M. S. Daw and M. I. Baskes, Phys. Rev. B **29**, 6443 (1984).
[25] P. Nordlander, S. Holloway, and J. K. Norskov, Surf. Sci. **136**, 59 (1984).
[26] S. G. Louie, Phys. Rev. Lett. **40**, 1525 (1978).
[27] S. G. Louie, Phys. Rev. Lett. **42**, 476 (1979).
[28] D. Tomanek, S. G. Louie, and C. T. Chan, Phys. Rev. Lett. **57**, 2594 (1986).
[29] D. Tomanek, Z. Sun, and S. G. Louie, Phys. Rev. B **43**, 4699 (1991).
[30] S. Wilke, D. Hennig, and R. Löber, Phys. Rev. B **50**, 2548 (1994).
[31] J. F. Paul and P. Sautet, Phys. Rev. B **53**, 8015 (1996).
[32] W. Dong, G. Kresse, J. Furthmüller, and J. Hafner, Phys. Rev. B **54**, 2157 (1996).
[33] A. Eichler, J. Hafner and G. Kresse, J. Phys. Condens. Matter **8**, 7659 (1996).
[34] B. Hammer and M. Scheffler, K. W. Jacobsen, and J. Norskov, Phys. Rev. Lett. **73**, 1400 (1994).
[35] J. A. White, D. M. Bird, M. C. Payne, and I. Stich, Phys. Rev. Lett. **73**, 1404 (1994).
[36] B. Hammer and M. Scheffler, Phys. Rev. Lett. **74**, 3487 (1995).
[37] B. Hammer and J. K. Norskov, Surf. Sci. **343**, 211 (1995).
[38] P. Kratzer, B. Hammer, and J. K. Norskov, Surf. Sci. **359**, 45 (1996).
[39] J. A. White, D. M. Bird, and M. C. Payne, Phys. Rev. B **53**, 1667 (1996).
[40] S. Wilke and M. Scheffler, Surf. Sci. **329**, L605 (1995).
[41] S. Wilke and M. Scheffler, Phys. Rev. B **53**, 4926 (1996).
[42] A. Eichler, G. Kresse, J. Hafner, Phys. Rev. Lett. **77**, 1119 (1996).

[43] A. Eichler, G. Kresse, J. Hafner, Surf. Sci. (to be published).
[44] G. Wiesenekker, G. J. Kroes, E. J. Baerends, and R. C. Mowrey, J. Chem. Phys. **102**, 3873 (1995).
[45] G. Wiesenekker, G. J. Kroes, and E. J. Baerends, J. Chem. Phys. **104**, 7344 (1996).
[46] A. Gross, B. Hammer, M. Scheffler, and W. Brenig, Phys. Rev. Lett. **73**, 3121 (1994).
[47] A. Gross, S. Wilke, and M. Scheffler, Phys. Rev. Lett. **75**, 2718 (1995).
[48] M. Kay, G. R. Darling, S. Holloway, J. A. White, and D. M. Bird, Chem. Phys. Lett. **245**, 311 (1995).
[49] G. Kresse and J. Hafner, Phys. Rev. B **47**, 558 (1993).
[50] G. Kresse and J. Hafner, Phys. Rev. B **48**, 13 115 (1993).
[51] G. Kresse and J. Furthmüller, Comput. Mater. Sci. **6**, 15 (1996).
[52] G. Kresse and J. Furthmüller, Phys. Rev. B **54**, 11 169 (1996).
[53] D. M. Ceperley and B. Alder, Phys. Rev. Lett. **45**, 566 (1980).
[54] J. P. Perdew and A. Zunger, Phys. Rev. B **43**, 5048 (1981).
[55] J. P. Perdew, J. A. Chevary, S. H. Vosko, K. A. Jackson, M. R. Pederson, D. J. Singh, and C. Fiolhais, Phys. Rev. B **46**, 6671 (1992).
[56] D. Vanderbilt, Phys. Rev. B **41**, 7892 (1990).
[57] G. Kresse and J. Hafner, J. Phys. Condens. Matter **6**, 8245 (1994).
[58] H. J. Monkhorst and J. D. Pack, Phys. Rev. B **13**, 5188 (1976).
[59] C. Kittel, *Introduction to Solid State Physics*, 6th ed. (Wiley, New York, 1986).
[60] R. Hoffmann, *Solids and Surfaces–A Chemist's View of Binding in Extended Structures* (VCH, 1988).
[61] R. Hoffmann, J. Phys. Condens. Matter **5**, A1 (1993).
[62] A. Eichler, G. Kresse, and J. Hafner, Surf. Sci. **346**, 300 (1995).